A novel discrete fracture networks model for multiphase flow in coal

Journal:	*Energy & Fuels*
Manuscript ID	ef-2022-03658p.R2
Manuscript Type:	Article
Date Submitted by the Author:	21-Dec-2022
Complete List of Authors:	Lu, Yuejian; China University of Geosciences Beijing Liu, Dameng; China University of Geosciences Beijing, Energy Resources Cai, Yidong; China University of Geosciences Beijing Zhou, Yingfang; University of Aberdeen, School of Engineering

A novel discrete fracture networks model for multiphase flow in coal

Yuejian Lu[a, b], Dameng Liu [a,b]*, Yidong Cai [a,b], Yingfang Zhou[c]

[a]*School of Energy Resources, China University of Geosciences, Beijing 100083, China*

[b]*Coal Reservoir Laboratory of National Engineering Research Center of CBM Development & Utilization, China University of Geosciences, Beijing 100083, China*

[c] *School of Engineering, Fraser Noble Building, King's College, University of Aberdeen, AB24 3UE Aberdeen, UK*

Abstract

Multiphase flow intensely affects the movement and accumulation of other fluids in coal, and plays an essential role in predicting the permeability of coal during coal bed methane (CBM) production. Fractures have played a decisive role in the transport of CBM after hydraulic fracturing has occurred. In this study, a multiscale pore network model (PNM) was constructed based on focused ion beam scanning electron microscopy (FIB-SEM) image results. Additionally, a novel discrete fracture network model — fracture-pore network model (F-PNM) was proposed to investigate the effect of fracture density, fracture developing direction and wettability on multiphase flow. The results reveal that the permeability of F-PNM increases with the increase of fracture density, which could be result of the predominance of snap off. The permeability decreases as the angle between the fracture and flow direction increases; initially, the permeability decreases steeply and then it tends to remain stable; for angles between 0° and 15°, the permeability decreased by as much as 61.8%. Moreover, the wettability of coal has limited impact on its water relative permeability; however, it has a measurable effect on gas relative permeability, which could be owing to water accumulation on the

coal surface under different wettability conditions. A good wetting performance would have a negative effect on the CBM production and reduce flow back efficiency.

Keyword: coalbed methane; pore network model; relative permeability; wettability

1. Introduction

With countries continuing to set energy saving and emission reduction targets, coal bed methane (CBM), an unconventional resource, can play an increasingly important role in the global energy structure by alleviating the energy shortage to some extent and contributes to mine safety and environmentally friendly[1–4]. CBM is stored in a state of absorption mainly in coal matrix nanopores, less than 100 nm in diameter with a small amount of it stored as free gas in coal cleats or fractures [5–7]. During CBM exploitation, methane first desorbs from the surfaces of coal matrix pores, and then migrates to the cleat system[8]. Because CBM recovery efficiency is predominantly influenced by the permeability of coal and gas-water distribution in coal[9,10], an insight into multiphase flow in coal would be important. Investigating the characteristics of multiphase flow in coal is difficult because of the strong heterogeneity of coal pore structure. Experiments and simulations are commonly used to study pours media. Gas/water relative permeability has been analyzed based on in situ dynamic micro-computed tomography imaging technology[11], Ma et al. studied the spontaneous imbibition of water using a nuclear magnetic resonance experiment[12], Zhao et al. stimulated relative permeability of two immiscible fluids flowing in a porous media using the lattice Boltzmann method[13]. Jing et al. simulated multiphysics gas flow in coal using a pore network

model (PNM) [8]. Unlike the experimental method and lattice Boltzmann method, PNMs are being widely used to quantitative characterize the pore structure of porous media and simulate fluid flow in them because of its high efficiency and high accuracy[14].

Coal being able to provide storage space for methane and serve as a transport channel for fluids, the degree of pore-fracture development in coal determines its permeability and connectivity[8,15]. Because of its two main advantages of PNM, namely, flexibility, efficiency and could visualize the fluid transport changes, thus it has become a interesting research topic in areas related to porous media[16–18]. The coordination number of connected pores increased with increasing pore diameter by Avizo simulation[19], indicating that larger pore tables appear to have better permeability. In contrast, the shape factor of pore decreases with increasing pore diameter, suggesting that the larger the pores are, the rougher the pore surface is [20]. In medium- and high-rank coals, the fluid pressure is more likely to reach equilibrium if differences among pressure in the X, Y and Z directions are not large[21]. Additionally, hydrate saturation affects the pore size distribution and pore network connectivity in coal[22], making the permeability of coal to change. Generally, the gas _phase permeability tends to decrease with increasing hydrate saturation[23]. The factors affecting fluid flow in an actual coal reservoir include curvature; ground stress; natural fracture development; desorption and contraction effects; and shape, roughness[24,25]. These factors are considered as much as possible when developing a PNM to enable the accurate reflection of the actual conditions of a coal seam.

Coal reservoirs in China are commonly known to have low porosity, low permeability, and high CBM adsorption[11,26,27]. Thus, the use of new technologies, including hydraulic fracturing technology, and the use of chemical methods, and microbially enhanced coalbed methane to improve the parameters of coal seam properties have become necessary[28–30]. However, investigating the effect of fractures by using a PNM for fluid flow simulations has always been a challenge. In this study, a PNM was constructed using focused ion beam scanning electron microscopy (FIB-SEM) images. A new method for adding several fractures to a PNM was also proposed to investigate the effect of fracture density, fracture direction, and wettability of coal on multiphase fluid flow in it using a fracture-pore network model (F-PNM).

2. F-PNM network model

2.1 Pore network model construction based on FIB-SEM images

Coal reservoir, composed of pores and fractures, is considered a dual pore system[31–33]. Characterizing the full-size pore structure of coal is difficult because of its low porosity, low permeability, and strong heterogeneity. Although mercury intrusion porosimetry can be used to measure coal pores whose radii fall in the range between 1.5 and 400 μm, the measurements made will not be accurate enough to characterize coal micropores and mesopores resulting from the deformation of the coal pore structure at high pressures. In a carbon dioxide and nitrogen adsorption experiment, only micropores and mesopores could be measured accurately at low pressures[34]. Because it has limited resolution, X-ray computed tomography can be used to observe coal fractures[35]. To build a matrix model, which is accurate and close to nature state, initially

a cubic nano-micro pore network is constructed (as shown in Figure 1a and Figure 1b), its pore radius, pore size distribution (PSD) is refer to the results of FIB-SEM in our previous work[36]. To maintain a balance between calculation accuracy and efficiency, 27000 pores and a cube with side lengths of 23.2 μm were constructed to study the characteristics of fluid flow in coal. As Figure 1c and 1d indicate, the PSDs of the samples, obtained using FIB-SEM and the PNM are similar, indicating that the developed PNM is acceptable. Table 1 presents the basic properties of the PNM used for simulating fluid flow in coal.

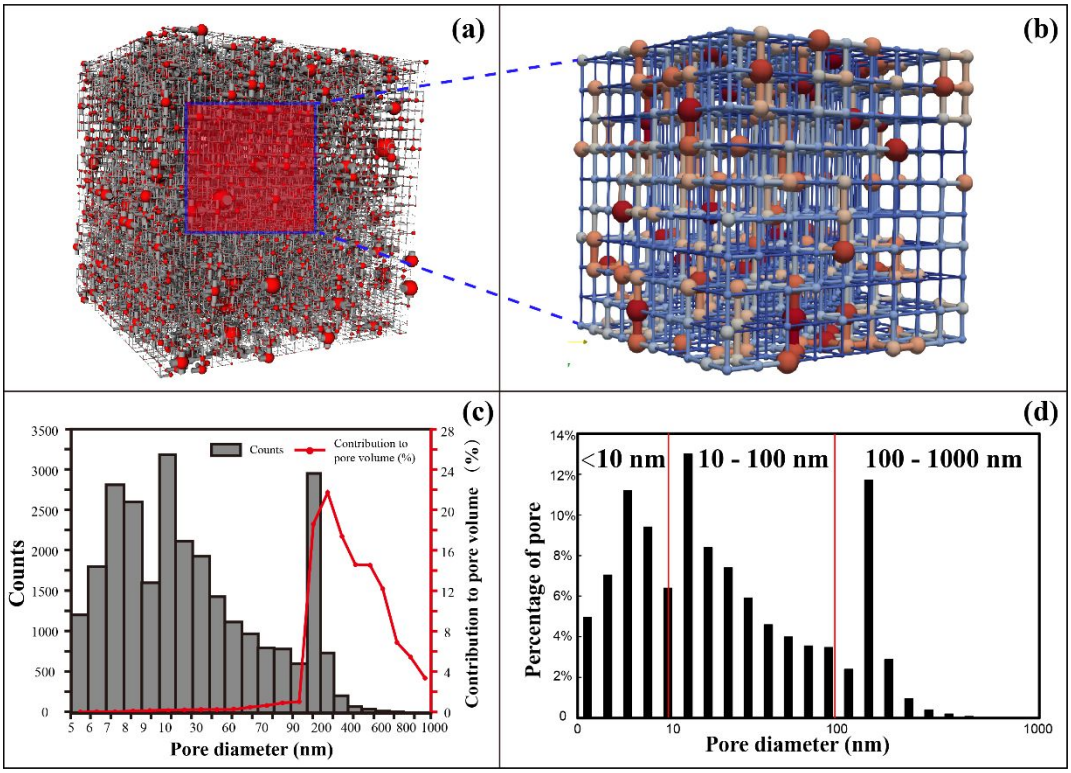

Figure 1. Pore network model of coal sample and pore size distribution. (a) Matrix PNM with 30 × 30 × 30 pores. (b) Pore and throat structure with small viewing angle, pores are shown as sphere with different colors, showing their radius, connected with throats; (c) Pore size distribution of FIB-SEM results from Li.et al. [Reproduced with permission from ref 36. Copyright 2017, Elsevier B.V.] (d) Pore size distribution of PNM in this work.

Table1 Basic properties of Pore Network model of coal matrix

Property	Value
Net porosity	1.62 %

Model dimensions	23.2 × 23.2 × 23.2 (μm)
Spacing of two consecutive pores	0.345 μm
Number of pores in 3 directions	[30, 30, 30]
Pore radius range	2 nm to 500 nm
Absolute permeability	1.01×10^{-5} mD
Invading gas phase	Methane
Gas temperature	400K

2.2 Discrete fracture network modeling

In this study, a F-PNM was built by modifying the developed PNM by adding one or more fractures, and the steps involved in building the F-PNM were as follows: the fracture was assumed to be an ellipse on a two-dimensional plane with its shape and size controlled by the semimajor axis (length = a), semiminor axis (length = b), fracture thickness (2h), major axis, minor axis, and fracture center coordinates. In the PNM, the fracture was represented by two pores (New_pore1 and New_pore2) and the throat (New_throat) connecting them. The radii of New_pore1 and New_pore2 were the same and equal to b, the length of New_throat was the distance between New_pore1 and New_pore2 minus the radius of each of the two pores, and the radius of New_throat was h. The schematic of the fracture model is presented in Figure 2.

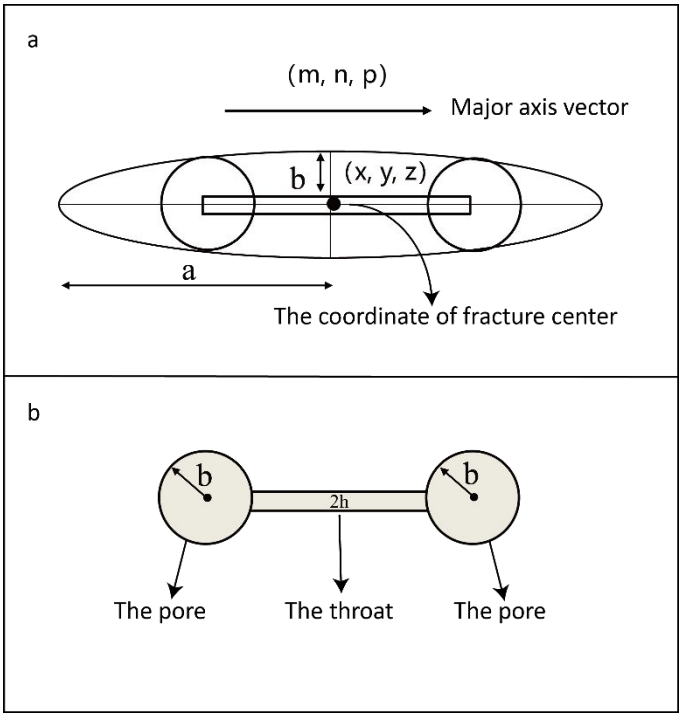

Figure 2 The schematic of fracture model. (a) original fracture shape;(b) simplified fracture shape

After building the fracture model, the coordinate numbers of New_pore1 and New_pore2 were updated based on the positional relationship between the fracture and pores in the original PNM. The detailed process involved in adding fracture to the pipe network was as the following steps:

（1） Reading original pores and throats data

（2） Reading candidate fracture data

（3） Looping the throats considered in Step (1)

（4） Judging the positional relationship between the candidate fracture and the two pores (pore1 and pore2) connected to the throat (throat1)

a) Both Pore1 and Pore2 are outside Throat1 and the fracture, the fracture is not crossed by Throat1, coordinate number of New_pore1 and New_pore2 remain unchanged.

b) Both Pore1 and Pore2 are outside Throat1 and the fracture, the fracture is crossed by Throat1, both Pore1 and Pore2 are considered as being connected to New_pore1 if the sum of the distances between Pore1 and

New_Pore 1 and Pore2 and New_Pore 1 is less than the sum of the distance between Pore1 and New_Pore 2 and Pore2 and New_Pore 2 , and if not both Pore1 and Pore2 are considered as being connected to New_pore2.

c) One pore (pore1) is inside the fracture and the other one (pore2) is outside the fracture, connecting the pore2 and New_Pore 1 or New_Pore 2 according the distance between pore1 and New_Pore 1 and New_Pore 2, and adding the coordinate number pore (New_Pore 1 or New_Pore 2) which connected to the pore2.

d) Both Pore1 and Pore2 are inside the fracture, the coordinate numbera of New_pore1 and New_pore2 remain unchanged, and Pore1, Pore2 and Throat1 are deleted.

(5) Adding a new throat between New_Pore 1 and New_Pore 2

(6) Calculating the hydraulic conductance of pipe elements.

The flow chat of constructing fracture-pore network model was presented in Figure 3

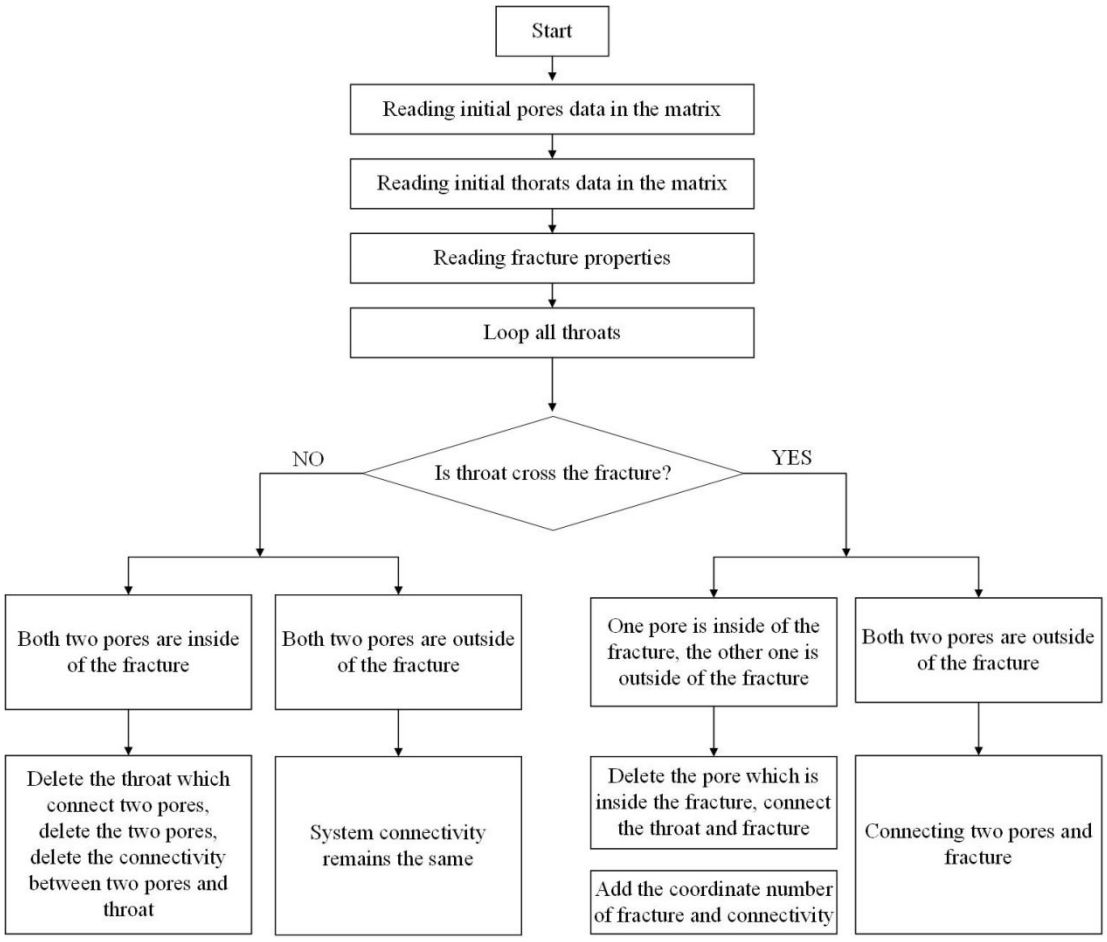

Figure 3. The flow chat of constructing fracture-pore network model

Figure 4 shows the fracture(s) Added to the PNM. As can be seen in figure, complex connection exits between the fracture and pores around it. More than one fracture can also be added to the F-PNM. The effect of the fracture on the fluid flow simulation in a porous medium could be determined by changing the properties of the fracture, including its direction, size, and wettability, et al.

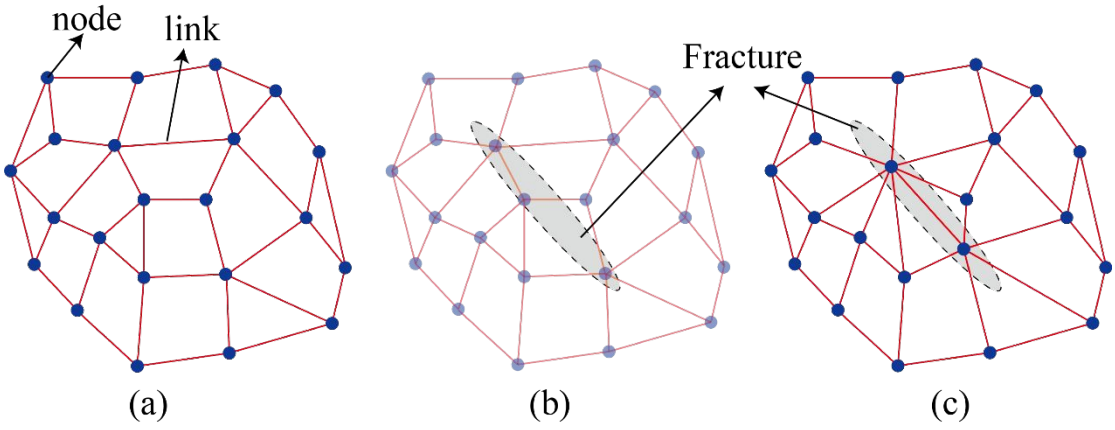

Figure 4. Add fracture in the F-PNM. (a) Original PNM;(b) The fracture is going to be added;(c)

Re-link the fracture with node in PNM

3. Fracture-pore network modeling of multiphase flow under wet conditions

3.1 Capillary entry pressure of the elements in the F-PNM

When gas flow simulation is performed using the F-PNM, the gas flow direction will depend on the driving force of the gas phase and the capillary force of the water. The capillary entry pressure of a throat in F-PNM can be calculated as follows:

$$P_{\text{entry}} = P_{\text{wetting}} - P_{\text{nonwetting}} = \frac{2\gamma}{r}\cos\theta \quad (1)$$

where γ is the interfacial tension among methane, water and coal sample, θ is the contact angle of coal, and r is the throat radius.

As mentioned in previous studies, the capillary entry pressure of an angular pore can be represented as follows[37]:

$$P_{\text{entry}} = \frac{\gamma(1+2\sqrt{\pi G})}{r} F_d(\theta,G) \quad (2)$$

$$F_d(\theta,G) = \frac{1+\sqrt{1+4G(\pi\left(1-\frac{3\theta}{\pi}\right)+3\sin\theta\cos\theta-\frac{\cos^2\theta}{4G})/\cos^2\theta}}{1+2\sqrt{\pi G}} \quad (3)$$

where G is the pore shape factor, which can be calculated using the following equation[38]:

$$G = \frac{S}{L^2} \quad (4)$$

where S is the cross-sectional area of the element and L is the perimeter length of the element.

3.2 Governing equations

In the F-PNM, the volume of fluid flowing into a pore is same, at that flowing out from a pore, indicating that fluid flow obeys mass conservation equation; for a given pressure, the total gas flow rate each pore can be calculated using the following equation [39]:

$$\sum_j q_{ij} = \sum_j g_{ij}(P_i - P_j) = 0 \quad (5)$$

where g_{ij} is the conductivity of the element, q_{ij} is the rate of the volumetric flow from Pore *i* to Pore *j*, P_i and Pj are the pressure at Pore *i* and Pore *j*, respectively. The fluid conductivity between any two pores is controlled by various factors, including the cross-sectional area of the element, viscosity of the fluid and shape factor of the element[40]. which could be calculated using the harmonic mean as given below.

$$\frac{L_{ij}}{g_{ij}} = \frac{L_i}{g_i} + \frac{L_t}{g_t} + \frac{L_j}{g_j} \tag{6}$$

where L_{ij} is the total length of element (sum of radius of the two pores and throat), L_i is the radius of Pore i, g_i is the conductivity of Pore i, L_j is the radius of Pore j, g_j is the conductivity of Pore j, L_t is the radius of the throat, g_t is the conductivity of the throat. The throat conductivity between the two pores is shown in Figure 5.

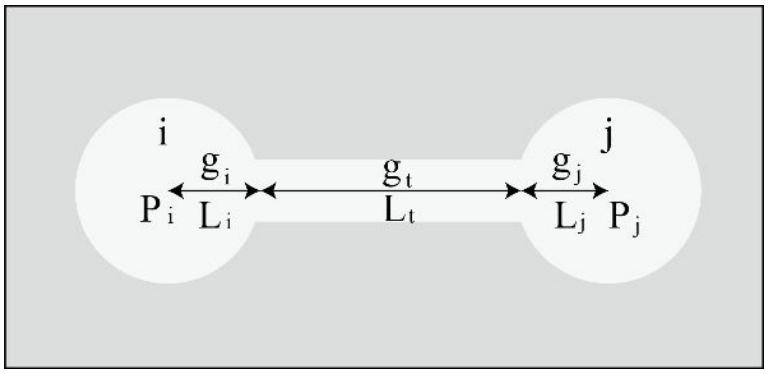

Figure 5. Conductivity of throat between two pores

Based on Eq (5) and Darcy's law, the gas permeability of PNM could be obtained by using the following equation:

$$K = \frac{Q_{\mathrm{m}} \bar{\mu} L}{A(P_{\mathrm{inlet}} - P_{\mathrm{outlet}})\rho_{\mathrm{avg}}} \tag{7}$$

where Q_{m} is the total single-phase flow rate, kg/s; A is the cross-sectional area in the flow direction, m^2;L is the length of the network, m; $(P_{\mathrm{inlet}} - P_{\mathrm{outlet}})$ is the pressure gradient of the network, Pa; and $\bar{\mu}$ and ρ_{avg} are the averages of viscosity (Pa·s) and density (kg/m^3) of the gas phase, respectively. For a two-phase flow (gas and liquid) through the pore network, gas/liquid relative permeability could be expressed as follows[41]:

$$K_g = \frac{Q_g}{Q_{\mathrm{m}}} \tag{8}$$

$$K_w = \frac{Q_w}{Q_{\mathrm{m}}} \tag{9}$$

where K_g is the gas relative permeability, Q_g is the total flow rate of gas, kg/s, K_w is the water relative permeability, and Q_g is the total water flow rate, kg/s.

To confirm the validity of the model, drainage simulation was performed as shown in Figure 6. In the figure, methane flows into the F-PNM under the driving force. When the capillary pressure is 554.9 psi, gas saturation is at low level (gas saturation is 5%); as the capillary pressure increased, gas flowed along the fracture, and then diffused around the fracture as shown in Figure 6b, Figure 6c, Figure 6d, and the capillary pressure being consistent with the controlling effect of the fracture on the fluid in natural state, the validity of the F-PNM was confirmed.

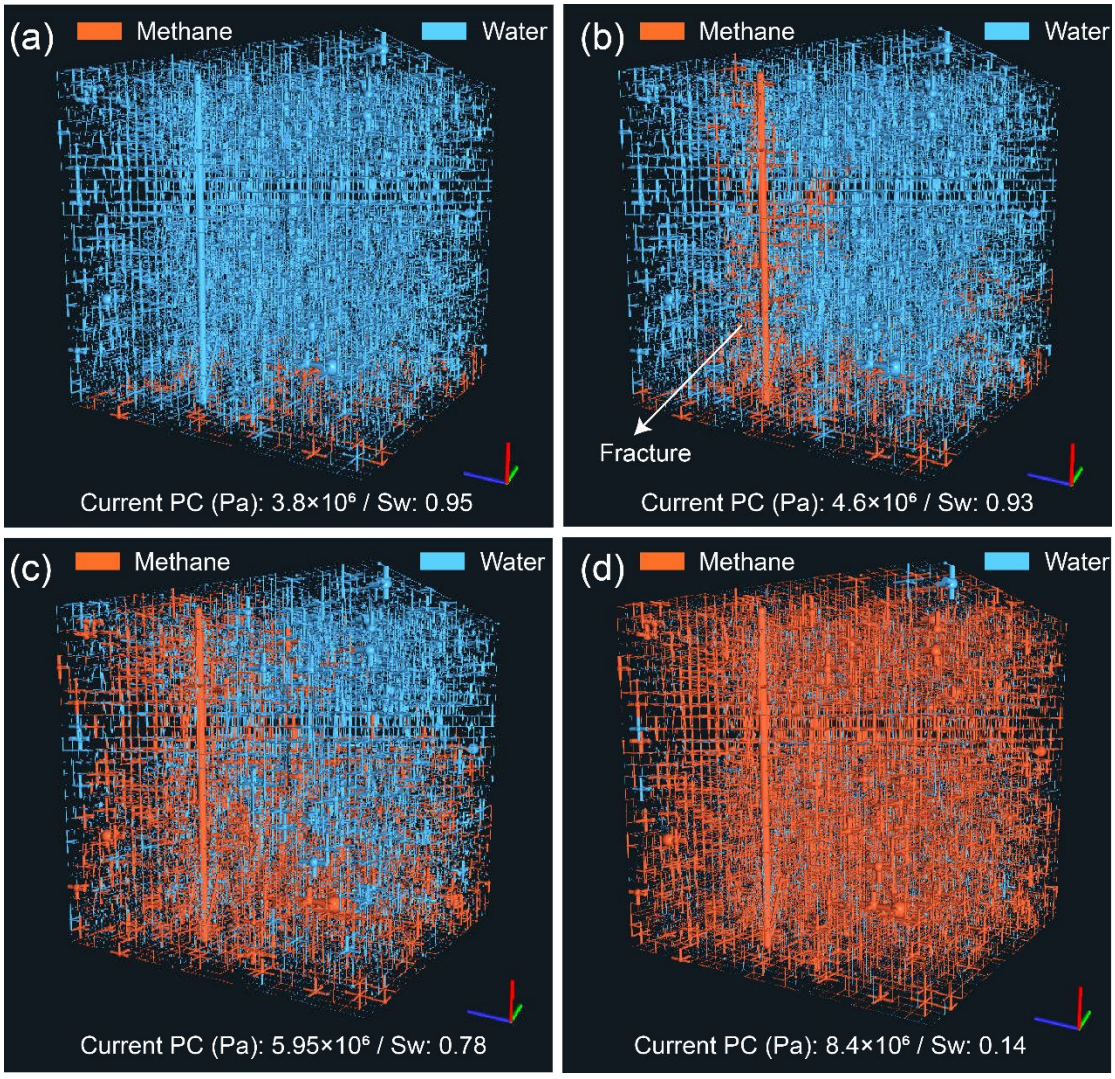

Figure 6. The process of drainage based on F-PNM, add 1 fracture. (a, capillary pressure= 3.8×10^6 Pa ; b, capillary pressure = 4.6×10^6 Pa; c, capillary pressure =5.95×10^6 Pa ; d, capillary pressure = 8.4×10^6 Pa)

4. Results and discussion

4.1 Effect of fracture density on fluid flow

To investigate the effect of the fracture number on coal permeability, six parallel fractures of the same scale were added to the PNM (Section 2.2). The fracture parameters are shown in Table 2. The variation of the permeability (obtained using the F-PNM) with the fracture number is illustrated in Figure 7. coal matrix increases as the fracture density increases, and the fracture improves the permeability. As fractures are added, the coal matrix permeability increases rapidly (from 1×10^{-5} to 2.57×10^{-5} mD) until the fracture number reaches four, and any further addition of fractures leads to only a slight change in the permeability. After the addition of six fractures, the coal matrix permeability quadruples, indicating that fractures play a key role in improving coal matrix permeability.

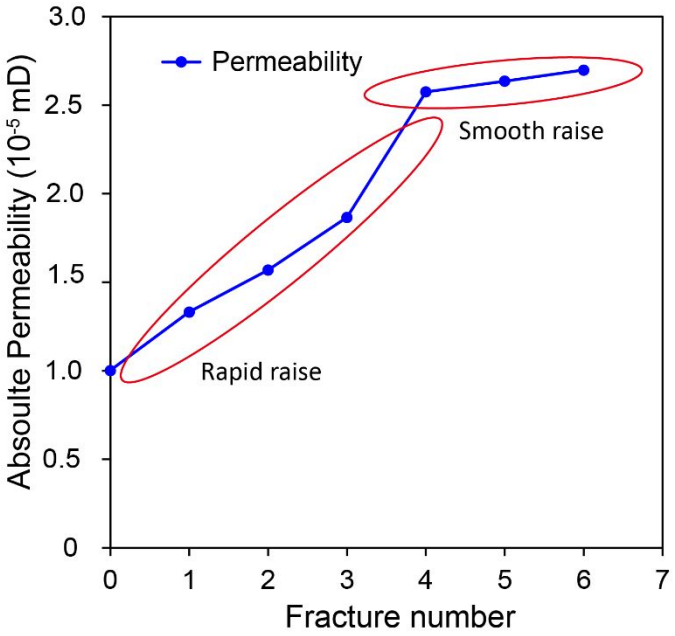

Figure 7. The relationship between absolute permeability of F-PNM and fracture number

Table 2 The scale and position of various fracture.

No.	Length of long axis	Length of short axis	Thinness	Center of fracture	Major axis vector	Minor axis vector
1	1×10^{-5}	8×10^{-7}	5×10^{-7}	(1.2×10^{-5}, $8e^{-7}$, 1.16×10^{-5})	(1,0,0)	(0,0,1)
2	1×10^{-5}	8×10^{-7}	5×10^{-7}	(1.2×10^{-5}, $5.6e^{-6}$, 1.16×10^{-5})	(1,0,0)	(0,0,1)
3	1×10^{-5}	8×10^{-7}	5×10^{-7}	(1.2×10^{-5}, $1.13e^{-5}$, 1.16×10^{-5})	(1,0,0)	(0,0,1)
4	1×10^{-5}	8×10^{-7}	5×10^{-7}	(1.2×10^{-5}, $1.68e^{-5}$, 1.16×10^{-5})	(1,0,0)	(0,0,1)
5	1×10^{-5}	8×10^{-7}	5×10^{-7}	(1.2×10^{-5}, $2.25e^{-5}$, 1.16×10^{-5})	(1,0,0)	(0,0,1)
6	1×10^{-5}	8×10^{-7}	5×10^{-7}	(1.2×10^{-5}, $9.6e^{-5}$, 1.16×10^{-5})	(1,0,0)	(0,0,1)

In addition, fractures density would affect relative permeability by changing the microscopic gas-water distribution. Figure 8 presents the relationship between gas/water relative permeability and saturation after several fractures have been added. The fracture number has a small effect on gas/water relative permeability. When it is less than 4, the gas/water relative permeability maintains the same trend and the saturation at the equal permeability point is in the range between 0.35 and 0.5, corresponding to a gas/water relative permeability of approximately 0.1. When the number of fractures added is four or more, the saturation at the equal permeability point is in the range between 0.5 and 0.6, corresponding to an increased relative permeability of 0.2. In a coal matrix, the fractures have a stronger conductivity than pores. As the fracture number continues to increase, the fracture coordination number also increases, leading to an improvement in coal matrix permeability. However, once the fracture number reaches a certain value, high water saturation would lead snap off to predominate, influencing the fluid flow capacity of gas/water in the porous medium[14]. When more than four fractures are added to the PNM, water saturation significantly increased and snap off starts to predominate, leading to a smooth increase in the gas permeability.

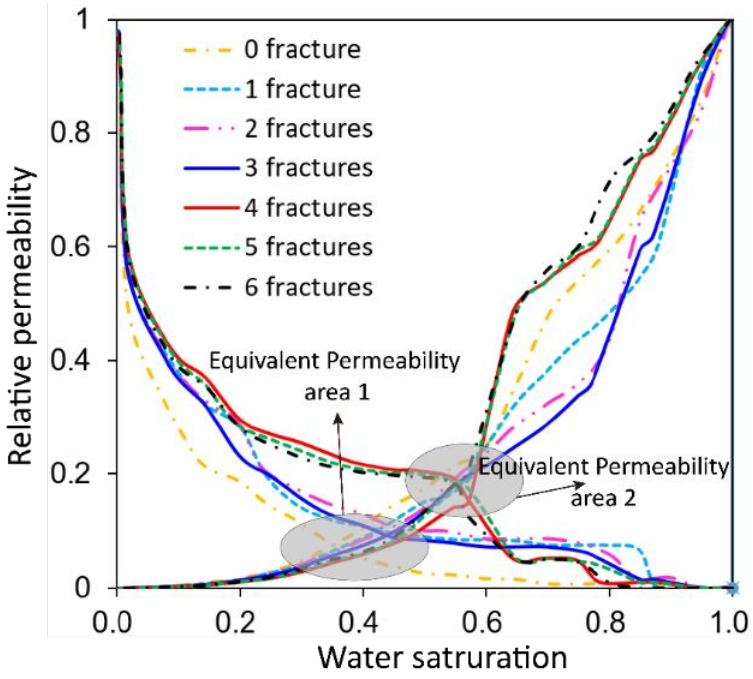

Figure 8. Relative permeability curves with different fracture counts

4.2 The effect of fracture direction on fluid flow

The dual pore-fracture system of a coal reservoir, which provides a transport channel and adsorption space for CBM, plays a critical role in improving coal reservoir permeability, thus increasing CBM production[42]. There is scarce study have examined on design of fracture distribution reasonably and efficiently in unconventional reservoir, especially in coal reservoir. In this study, we investigated the effect of fracture direction on the fluid flow using an F-PNM; in the model, the fracture direction represented the angle between fluid flow direction and fracture semimajor axis as shown in Figure 9a. To control other variables, different directions of eight fractures of the same scale were added to the pore network. Fracture data are presented in Table 3. Before simulating the fluid flow, the F-PNM was assumed to be water wet, and water/gas contact angle was set at 30°. Figure 9a shows the simulation results of the relationship between fracture direction and absolute permeability obtained using the PNM. According to the figure, the percolation flow capacity is highest when the fracture direction is parallel to the flow direction, and the absolute permeability is minimum when the fracture

direction is vertical to the flow direction. The permeability decreases as the angle between the fracture and flow direction increases; it decreases steeply at first and becomes steady later. When the angle between the fracture and flow directions is between 0° and 15°, the permeability decreases from 3.22×10^{-5} to 1.23×10^{-5} mD, a decrease of almost 61.8%; which decreases slightly as angle increases from 15°–90°, fell by only 12.1%. Previous scholar found similar result based on Finite Element Analyses method[43], different from this work, the permeability decreased less when the fracture direction changed from 0° to 30° , as shown in Figure 9b, which is mainly related to the number of model elements, in general, the more complex the model elements, the higher the calculation accuracy.

Table 3 The scale and direction of various fracture.

No.	Center of fracture	Major axis vector	Major axis vector	Angle	Permeability (10^{-5} mD)
1	(1.2×10^{-5}, 1.2×10^{-5}, 1.2×10^{-5})	(0,1,0.27)	(0,0,1)	0	3.22
2	(1.2×10^{-5}, 1.2×10^{-5}, 1.2×10^{-5})	(0,1,0.58)	(0,0,1)	10	1.45
3	(1.2×10^{-5}, 1.2×10^{-5}, 1.2×10^{-5})	(0,1,0.27)	(0,0,1)	15	1.23
4	(1.2×10^{-5}, 1.2×10^{-5}, 1.2×10^{-5})	(0,1,0.58)	(0,0,1)	30	1.20
5	(1.2×10^{-5}, 1.2×10^{-5}, 1.2×10^{-5})	(0,1,1)	(0,0,1)	45	1.18
6	(1.2×10^{-5}, 1.2×10^{-5}, 1.2×10^{-5})	(1,0,0)	(0,0,1)	60	1.14
7	(1.2×10^{-5}, 1.2×10^{-5}, 1.2×10^{-5})	(1,0,0)	(0,0,1)	75	1.10
8	(1.2×10^{-5}, 1.2×10^{-5}, 1.2×10^{-5})	(1,0,0)	(0,0,1)	90	1.08

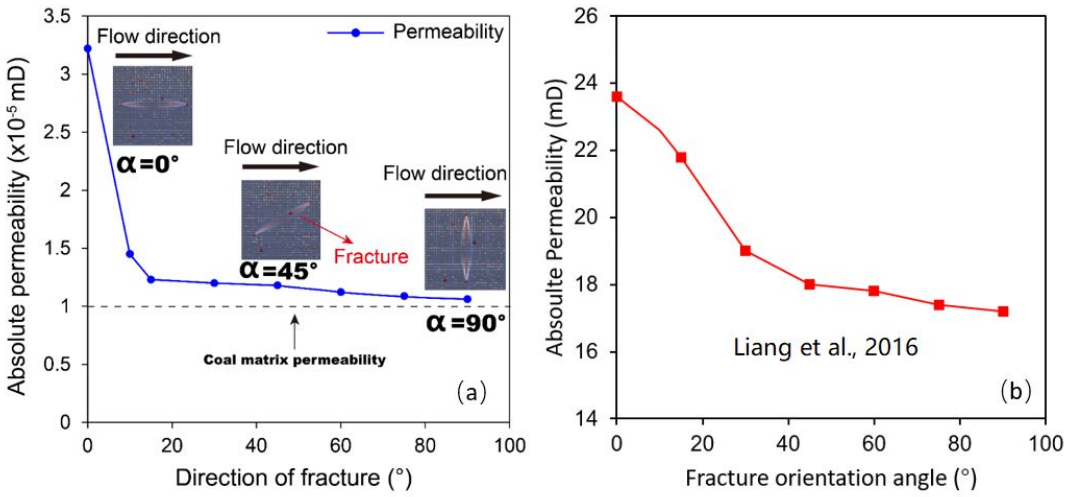

Figure 9. The relationship between the direction of fracture and permeability of F-PNM. (a) results

from F-PNM, (b) results from Liang et al. [Reproduced with permission from ref 43. Copyright 2016, Elsevier B.V.]

As Figure 10 shows, the gas flow capacity values for fracture directions of 0°, 15°, and 90° differ considerably. When a fracture parallel to the direction of fluid flow is the main transport pathway for gas, the gas relative permeability remains at a high level over a wide range of water saturation levels. However, only slight differences exist among the gas/water relative permeability values at fracture directions of 15°and 90°, which indicates that the fracture direction could have a direct effect on CBM production efficiency and that artificial fractures should be so designed that they are parallel to the fluid flow direction as much as possible when hydraulic fracturing occurs.

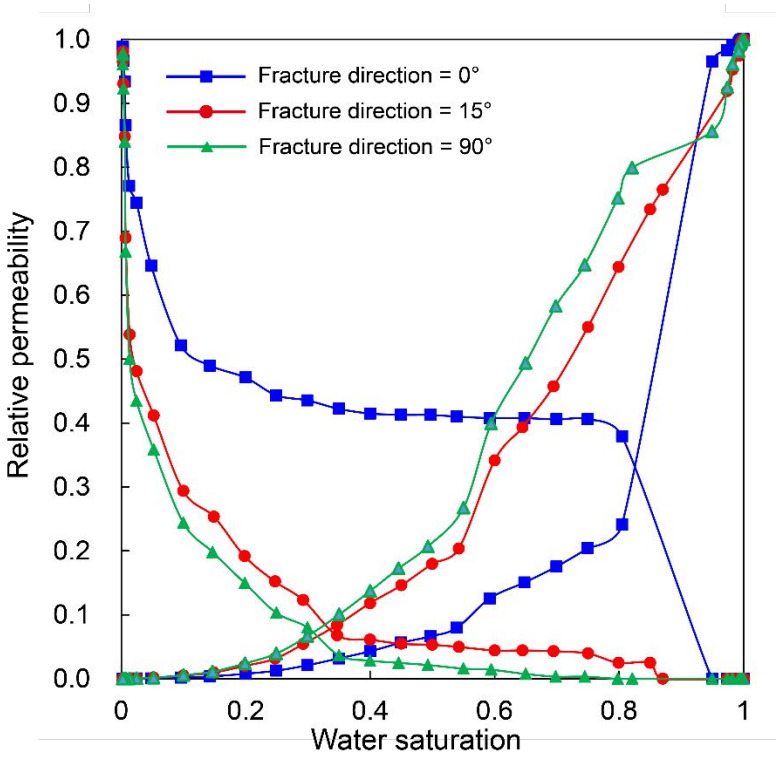

Figure 10. Relative permeability curves of F-PNM with adding different direction fracture

4.3 Effect of wettability on fluid flow

We also studied the effect of wettability of a porous medium on fluid flow during the drainage process using the F-PNM. The F-PNM was assumed to be hydrophilic with a contact angle between 10° and 80°. The wettability was assumed to be homogeneous,

and thus mixed wetting was not possible. The simulated curves displayed the same trends under different wettability conditions as shown in Figure 11. During the process of water saturation decrease from 100% to 0%, the capillary pressure increased rapidly with the decrease of water saturation, and then tend to be stable, when water saturation is less than 15%, it rises rapidly again. The stronger the wettability of a porous medium is, the lager the capillary pressure is. During the process of hydraulic fractures in drilling wells for extracting CBM, the methane flow direction depends on the pressure difference between gas and water, especially in nanopores with strong capillary pressure, water locking effect would be more obvious with the improved wetting performance, and result in reducing the efficiency of flow-back when using hydraulic fracturing technology.

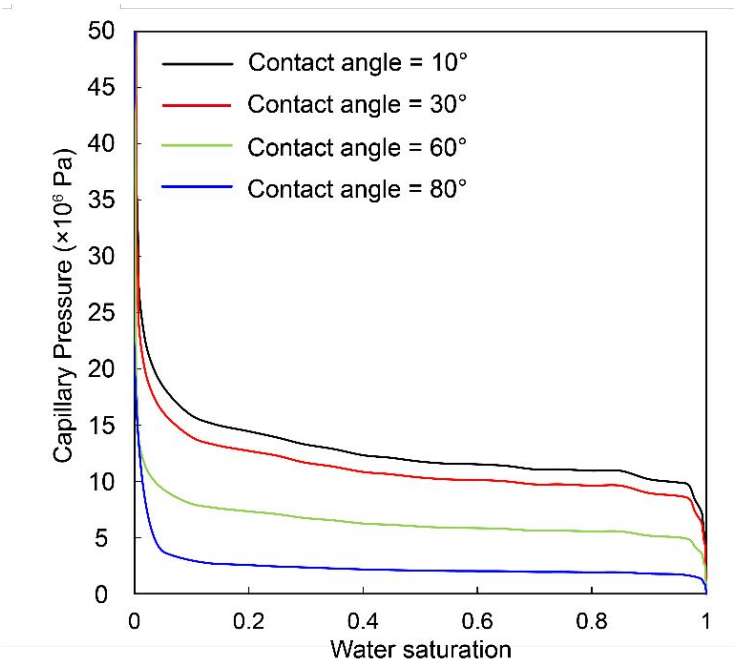

Figure 11. The relationship between capillary pressure and water saturation under different wettability of F-PNM

The water/gas relative permeability and water saturation curves shown in Figure 12 reveal that water/gas relative permeability increases gradually with the increase in the contact angle. There are stronger intermolecular forces between water molecular and solid as porous medium become more hydrophilic, which result in larger slip length and the smaller viscosity for fluid flow[44,45], and wreaked water flow capacity. By

comparing with pervious results based on experiment [46], the effect of wettability on gas relative permeability has the similar trends, however, water relative permeability curve is different under different wettability, the reason for this may be that there is difference in pore-fracture structure between F-PNM and coal sample, the irreducible water causes a less obstacle to water flow than to gas flow[47]. According to our simulation results, wettability has only a little effect on water relative permeability but a measurable effect on gas relative permeability, especially when water saturation is below 40%; this behavior of wettability could have been caused by small pores or throats, which would allow water accumulation in a hydrophilic porous medium and cause a negative effect on water flow[48]. Thus, strong water-wet coal reservoirs do not positively contribute to the CBM flow in pores or fractures, which would reduce the CBM production efficiency.

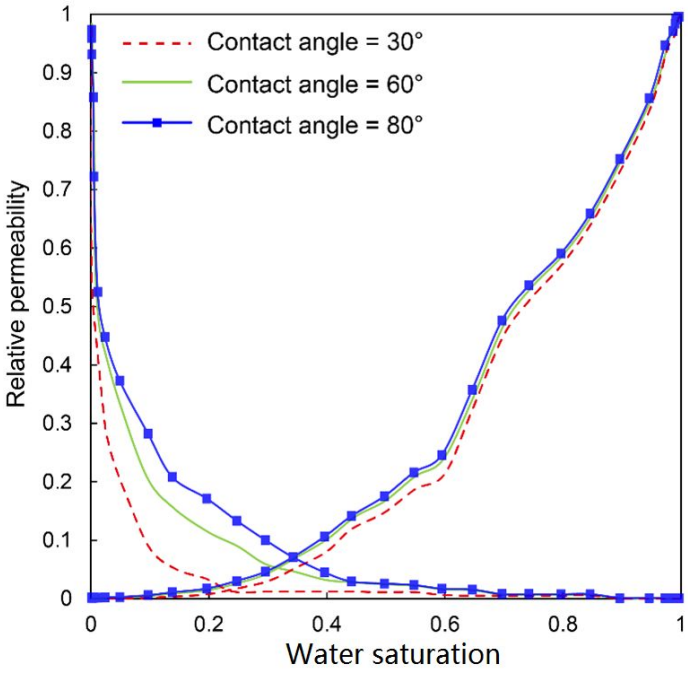

Figure 12. Relative permeability curves of F-PNM under different wettability

5. Conclusions

A PNM can be effectively used to determine the fluid flow mechanism in a porous medium. Complicated processes are involved in coal reservoir formation and the coal

pore fractures have strong heterogeneity; therefore, A F-PNM was constructed based on the structural characteristics of actual coal reservoirs. In this study, the effect of fracture density, fracture direction, and wettability of coal on fluid flow were explored using the F-PNM. However, the F-PNM we developed has some limitations: it does not consider the effect of gravity on fluid flow and it has mixed wettability; addressing of these limitations should be a priority of future researchers. Based on the study findings, the following conclusions can be drawn:

1) PNM with 23.2 × 23.2 × 23.2 (μm) was constructed based on FIB-SEM images of coal samples, meanwhile, a new method of adding a fracture into pore network model was proposed, which provides an efficient framework for investigating multiphase flow in both coal matrix and fractures.
2) When fracture density less than 4 per12487μm^3, the absolute permeability of F-PNM increases rapidly, and with the increase of fracture density, the permeability followed by insignificant change, which may be a result of the predominance of snap off. Additionally, fractures density would affect relative permeability by changing the microscopic gas-water distribution, as fractures density increases, the water-gas relative permeability increases.
3) The F-PNM permeability declines as the angle between the directions of the fracture and fluid flow increases, declining steeply at first and then becoming stable. For angles between 0° and 15°, the permeability declines by almost 61.8%. Moreover, the fracture parallel to fluid direction can significantly improve CBM relative permeability during CBM drainage.
4) While wettability of coal has only a limited impact on its water relative permeability, it has a measurable effect on its gas relative permeability, which may be mainly related to water accumulation on pores surfaces under different wettability conditions; moreover, good wetting performance would result in reducing the flow-back efficiency and cause a negative effect on CBM production.

Conflicts of Interest

Corresponding author

Phone: +86-10-82323971. Fax: +86-10-82326850. E-mail address: dmliu@cugb.edu.cn.

Notes

The authors declare no competing financial interest.

Acknowledgments

This research was funded by the National Natural Sciences Foundation of China (Grant No. 41830427, 41922016, 42130806), and financial support from China Scholarship Council (No. 202006400048).

References

(1) Cai, Y. D.; Li, Q.; Liu, D. M.; Zhou, Y. F.; Lv, D. W. Insights into matrix compressibility of coals by mercury intrusion porosimetry and N2 adsorption. *Int. J. Coal. Geol*. 2018, 200, 199-212.

(2) Zhou, S. D.; Liu, D. M.; Cai, Y. D.; Yao, Y. B.; Li, Z. T. 3D Characterization and quantitative evaluation of pore-fracture networks of two Chinese coals using FIB-SEM tomography. *Int. J. Coal. Geol*. 2017, 174, 41-54.

(3) Vishal, V.; Singh, T. N.; Ranjith, P. G. Influence of sorption time in CO2-ECBM process in Indian coals using coupled numerical simulation. *Fuel* 2015, 139, 51- 58.

(4) Roslin, A.; Pokrajac, D.; Wu, K.J.; Zhou, Y. F. 3D pore system reconstruction using nano-scale 2D SEM images and pore size distribution analysis for intermediate rank coal matrix. *Fuel* 2020, 275, 117934.

(5) Cai, Y.; Pan, Z.; Liu, D.; Zheng, G.; Tang, S.; Connell, L. D.; Yao, Y.; Zhou, Y. Effects of pressure and temperature on gas diffusion and flow for primary and enhanced coalbed methane recovery. *Energy Explor. Exploit*. 2014, 32 (4) 601- 619.

(6) Zhang, X. G.; Ranjith, P. G.; Perera, M. S. A.; Ranathunga, A. S.; Haque, A. Gas transportation and enhanced coalbed methane recovery processes in deep coal seams: a review. *Energy Fuels* 2016, 30 (11), 8832-8849.

(7) Liu, D. M.; Yao, Y. B.; Chang, Y. H. Measurement of adsorption phase densities with respect to different pressure: Potential application for determination of free and adsorbed methane in coalbed methane reservoir. *Chem. Eng. J.* 2022, 446, 137103.

(8) Jing, Y.; Rabbani, A.; Armstrong, R. T.; Wang, J.; Mostaghimi, P. A hybrid fracture-micropore network model for multiphysics gas flow in coal. *Fuel* 2020, 281, 118687.

(9) Clarkson, C. R.; Rahmanian, M.; Kantzas, A.; Morad, K. Relative permeability of CBM reservoirs: controls on curve shape. *Int. J. Coal. Geol.* 2011, 88 (4), 204-217.

(10) Keshavarz, A.; Yang, Y.; Badalyan, A.; Johnson, R.; Bedrikovetsky, P. Laboratory-based mathematical modelling of graded proppant injection in CBM reservoirs. *Int. J. Coal. Geol.* 2014, 136, 1- 16.

(11) Lu, Y. J; Liu, D. M.; Cai, Y. D; Li, Q.; Zhou, Y. F. Spontaneous imbibition in coal with in-situ dynamic micro-CT imaging. *J. Pet. Sci. Eng.* 2022, 208, 109296.

(12) Ma, Y. K; Deng, Z. M; Yue, J. W; Zhao, A. H; Hu, M. Y; Shen, L.Y. Nuclear magnetic resonance experiment on the influence of confining pressure on spontaneous imbibition of water in coal. *Energy Fuels* 2022, 36 (9), 4818-4829.

(13) Zhao, H. W.; Ning, Z. F.; Kang, Q. J.; Chen, L.; Zhao, T.Y. Relative permeability of two immiscible fluids flowing through porous media determined by lattice Boltzmann method. *Int. Commun. Heat Mass Transfer* 2017, 85, 53-61.

(14) He, M. X.; Zhou, Y. F.; Chen, B. T.; Zhang, T.; Wu, K. L.; Feng, D.; Li, X. F. Effect of pore structure on slippage effect in unsaturated tight formation using pore network model. *Energy Fuels* 2021, 35 (7), 5789-5800.

(15) Jia, Q. F.; Liu, D. M.; Ni, X. M.; Cai, Y. D.; Lu, Y. J.; Li, Z. Y.; Zhou, Y.F. Interference mechanism in coalbed methane wells and impacts on infill adjustment for existing well patterns. *Energy Rep.* 2022, 8, 8675-8689.

(16) Xu, Y.; Lun, Z. M.; Pan, Z. J.; Wang, H. T.; Zhou, X.; Zhao, C. P.; Zhang, D.F. Occurrence space and state of shale oil: A review. *J. Pet. Sci. Eng.* 2022, 211.

(17) Fu, X. X.; Zhao, C. P.; Lun, Z.M.; Wang, H.T.; Wang, M.; Zhang, D.F. Influences of controlled microwave field radiation on pore structure, surface chemistry and adsorption capability of gas-bearing shales. *Mar. Pet. Geol.* 2021, 130 (727), 105134.

(18) Jia, Q. F.; Liu, D. M.; Cai, Y. D.; Fang, X. L.; Li, L. J. Petrophysics characteristics of coalbed methane reservoir: A comprehensive review. *Front. Earth Sci.* 2021, 15 (2), 202-223.

(19) Shi, X. H.; Pan, J. N.; Pang, L. L.; Wang, R.; Li, G. F.; Tian, J. J.; Wang, H. C. 3D microfracture

network and seepage characteristics of low-volatility bituminous coal based on nano-CT. *J. Nat. Gas Sci. Eng.* 2020, 83, 103556.

(20) Jia, Q. F.; Liu, D. M.; Cai, Y. D.; Zhou, Y. F.; Zhao, Z.; Yang, Y. AFM characterization of physical properties in coal adsorbed with different cations induced by electric pulse fracturing. *Fuel* 2022, 327, 125247.

(21) Jia, Q. F.; Liu, D. M.; Cai, Y. D.; Lu, Y. J.; Li, R.; Wu, H.; Zhou, Y. F. Nano-CT measurement of pore-fracture evolution and diffusion transport induced by fracturing in medium-high rank coal. *J. Nat. Gas Sci. Eng.* 2022, 106, 104769.

(22) Luo, Y. J.; Sun, Y. S.; Li, L. J.; Wang, X.; Qin, C. Z.; Liu, L. L.; Liu, C. L.; Wu, D. Y. Image-based pore-network modeling of two-phase flow in hydrate-bearing porous media. *Energy* 2022, 252, 124044.

(23) Lanetc, Z.; Zhuravljov, A.; Jing, Y.; Armstrong, R. T.; Mostaghimi, P. Coupling of transient matrix diffusion and pore network models for gas flow in coal. *J. Nat. Gas Sci. Eng.* 2021, 88, 103741.

(24) Fu, X. X.; Lun, Z. M.; Zhao, C.P.; Zhou, X.; Wang, H.T.; Zhou, X.T.; Xu, Y.; Zhang, H.; Zhang, D.F. Influences of controlled microwave field irradiation on physicochemical property and methane adsorption and desorption capability of coals: Implications for coalbed methane (CBM) production. *Fuel* 2021, 301, 121022.

(25) Zhao, Y.L. long; Wang, Z. M.; Ye, J. P.; Sun, H. S.Y.; Gu, J. Y. Lattice Boltzmann simulation of gas flow and permeability prediction in coal fracture networks. *J. Nat. Gas Sci. Eng.* 2018, 53, 153-162.

(26) Yao, Y. B; Liu, D. M.; Cai, Y. D.; Li, J. Q. Advanced characterization of pores and fractures in coals by nuclear magnetic resonance and X-ray computed tomography. *Sci. China Earth Sci.* 2010, 53 (6), 854-862.

(27) Men, X. Y.; Tao, S.; Liu, Z. X.; Tian, W. G.; Chen, S. D. Experimental study on gas mass transfer process in a heterogeneous coal reservoir. *Fuel Process. Technol.* 2021, 216, 106779.

(28) Zhang, D.; He, H.; Ren, Y.; Haider, R.; Urynowicz, M.; Fallgren, P. H.; Jin, S.; Ishtiaq Ali, M.; Jamal, A.; Adnan Sabar, M.; et al. A mini review on biotransformation of coal to methane by enhancement of chemical pretreatment. *Fuel* 2022, 308, 121961.

(29) Zhao, W. Z.; Su, X. B.; Xia, D. P.; Hou, S. H.; Wang, Q.; Zhou, Y. X. Enhanced coalbed methane recovery by the modification of coal reservoir under the supercritical CO2 extraction and anaerobic digestion. *Energy* 2022, 259, 124914.

(30) Ahamed, M. A. A.; Perera, M. S. A.; Dong-yin, L.; Ranjith, P. G.; Matthai, S. K. Proppant damage mechanisms in coal seam reservoirs during the hydraulic fracturing process: A review. *Fuel* 2019, 253, 615- 629.

(31) Ouyang, Z. Q.; Liu, D. M.; Cai, Y. D.; Yao, Y. B. Fractal analysis on heterogeneity of pore-fractures in middle–high rank coals with NMR. *Energy Fuels* 2016, 30 (7), 5449-5458.

(32) Cai, Y. D; Liu, D. M; Pan, Z. J; Yao, Y. B; Li, J. Q; Qiu, Y. K. Pore structure and its impact on CH4 adsorption capacity and flow capability of bituminous and subbituminous coals from Northeast China. *Fuel* 2013, 103, 258- 268.

(33) Liu, D. M.; Zou, Z.; Cai, Y. D.; Qiu, Y. K.; Zhou, Y. F.; He, S. An updated study on CH4 isothermal adsorption and isosteric adsorption heat behaviors of variable rank coals. *J. Nat. Gas Sci. Eng.* 2021, 89, 103899.

(34) Yang, S.G.; Yu, Q.C. Experimental investigation on the movability of water in shale nanopores: A case study of Carboniferous shale from the Qaidam Basin. *China. Res.* 2020, 56 (8), 1-23.

(35) Liu, D. M.; Zhao, Z.; Cai, Y. D.; Sun, F. R.; Zhou, Y. F. Review on applications of X-Ray computed tomography for coal characterization: recent progress and perspectives. *Energy Fuels* 2022, 36 (13), 6659-6674.

(36) Li, Z. T.; Liu, D. M.; Cai, Y. D.; Ranjith, P. G.; Yao, Y. B. Multi-scale quantitative characterization of 3-D pore-fracture networks in bituminous and anthracite coals using FIB-SEM tomography and X-ray μ-CT. *Fuel* 2017, 209, 43-53.

(37) Oren, P.-E.; Bakke, S.; Arntzen, O. J. Extending predictive capabilities to network models. *SPE J.* 1998, 3, 324- 336.

(38) Zhao, J. L.; Qin, F. F.; Derome, D.; Carmeliet, J. Simulation of quasi-static drainage displacement in porous media on pore-scale: Coupling lattice Boltzmann method and pore network model. *J. Hydrol.*2020,588,125080.

(39) Bakke, S.; Øren, P. E. 3-D pore-scale modelling of sandstones and flow simulations in the pore networks. *SPE J.* 1997, 2 (2), 136-149.

(40) Mason, G.; Morrow, N. R. Capillary behavior of a perfectly wetting liquid in irregular triangular tubes. *J. Colloid Interface Sci.* 1991, 141 (1), 262-274.

(41) Yang, L.; Ai, L.; Xue, K.H.; Ling, Z.; Li, Y. H. Analyzing the effects of inhomogeneity on the

permeability of porous media containing methane hydrates through pore network models combined with CT observation. *Energy* 2018, 163, 27-37.

(42) Cui, J.; Liu, D. M.; Cai, Y.D.; Pan, Z. Z.; Zhou, Y. F. Insights into fractures and minerals in subbituminous and bituminous coals by FESEM-EDS and X-ray μ-CT. *Fuel* 2019, 237, 977-988.

(43) Liang, B.; Jiang, H. Q.; Li, J. J.; Gong, C.C. A systematic study of fracture parameters effect on fracture network permeability based on discrete-fracture model employing Finite Element Analyses. *J. Nat. Gas Sci. Eng.* 2016, 28, 711-722.

(44) Su, Y. L.; Xu, J. L.; Wang, W. D.; Wang, H.; Zhan, S. Y. Relative permeability estimation of oil−water two-phase flow in shale reservoir. *Pet. Sci.* 2022, 1153–1164.

(45) Lu, Y. J.; Liu, D. M.; Cai, Y. D.; Gao, C. J.; Jia, Q. F.; Zhou, Y. F. AFM measurement of roughness, adhesive force and wettability in various rank coal samples from Qinshui and Junggar basin, China. *Fuel* 2022, 317, 123556.

(46) Sevket Durucan; Mustafa Ahsan; Shi, Ji, Q.; Amer Syed; Anna Korre; Two phase relative permeabilities for gas and water in selected European coals. *Fuel* 2014, 134(15), 226-236.

(47) Zhang, Z.; Yan., D. T.; Yang, S. G.; Zhang, X. G.; Li, G, Q.; Wang, G.; Wang, X, M.; Experimental studies on the movable-water saturations of different-scale pores and relative permeability of low-medium rank coals from the Southern Junggar Basin. *J. Nat. Gas Sci. Eng.* 2020, 83, 103585.

(48) Liu, D. M.; Yao, Y. B.; Yuan, X. H.; Yang, Y. B. Experimental evaluation of the dynamic water-blocking effect in coalbed methane reservoir. *J. Pet. Sci. Eng.* 2022, 217, 110887.

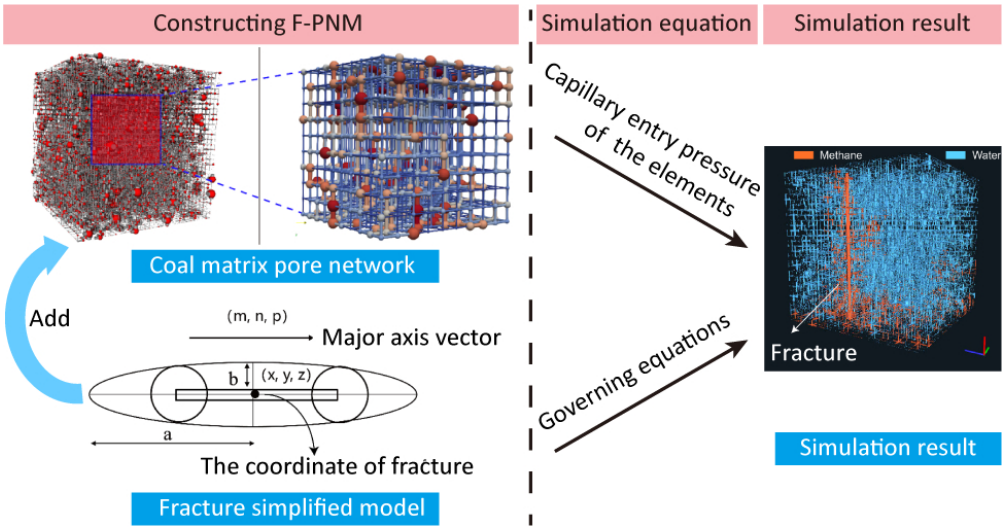

82x43mm (300 x 300 DPI)